Environmental Science
Water Research & Technology

ROYAL SOCIETY OF CHEMISTRY

PAPER

View Article Online
View Journal

Cite this: DOI: 10.1039/c9ew00834a

Functionalized electrospun polymer nanofibers for treatment of water contaminated with uranium†

Adam Johns,[a] Jiajie Qian,[a] Margaret E. Carolan,[a] Nabil Shaikh,[b] Allison Peroutka,[c] Anna Seeger,[a] José M. Cerrato,[b] Tori Z. Forbes *[d] and David M. Cwiertny *[ace]

Uranium (U) contamination of drinking water often affects communities with limited resources, presenting unique technology challenges for U^{6+} treatment. Here, we develop a suite of chemically functionalized polymer (polyacrylonitrile; PAN) nanofibers for low pressure reactive filtration applications for U^{6+} removal. Binding agents with either nitrogen-containing or phosphorous-based (*e.g.*, phosphonic acid) functionalities were blended (at 1–3 wt%) into PAN sol gels used for electrospinning, yielding functionalized nanofiber mats. For comparison, we also functionalized PAN nanofibers with amidoxime (AO) moieties, a group well-recognized for its specificity in U^{6+} uptake. For optimal N-based (Aliquat® 336 or Aq) and P-containing [hexadecylphosphonic acid (HPDA) and bis(2-ethylhexyl)phosphate (HDEHP)] binding agents, we then explored their use for U^{6+} removal across a range of pH values (pH 2–7), U^{6+} concentrations (up to 10 μM), and in flow through systems simulating point of use (POU) water treatment. As expected from the use of quaternary ammonium groups in ion exchange, Aq-containing materials appear to sequester U^{6+} by electrostatic interactions; while uptake by these materials is limited, it is greatest at circumneutral pH where positively charged N groups bind negatively charged U^{6+} complexes. In contrast, HDPA and HDEHP perform best at acidic pH representative of mine drainage, where surface complexation of the uranyl cation likely drives uptake. Complexation by AO exhibited the best performance across all pH values, although U^{6+} uptake *via* surface precipitation may also occur near circumneutral pH values and at high (10 μM) dissolved U^{6+} concentrations. In simulated POU treatment studies using a dead-end filtration system, we observed U removal in AO-PAN systems that is insensitive to common co-solutes in groundwater (*e.g.*, hardness and alkalinity). While more research is needed, our results suggest that only 80 g (about 0.2 lbs.) of AO-PAN filter material would be needed to treat an individual's water supply (contaminated at ten-times the U.S. EPA maximum contaminant level for U) for one year.

Received 20th September 2019,
Accepted 9th December 2019

DOI: 10.1039/c9ew00834a

rsc.li/es-water

Water impact

Resource-constrained communities that rely on unregulated water supplies often have limited access to appropriate treatment technologies. Uranium contamination poses a particular challenge for many such communities in the Southwestern United States from legacy mining activities. Here, using insights from uranium extraction efforts, we produce nanotechnology-enabled filtration materials tailored for uranium removal under conditions suitable for point-of-use treatment.

Introduction

Uranium (U) contamination affects the drinking water of many consumers in the Four Corners region of the United States (Colorado, New Mexico, Arizona, and Utah), including indigenous communities such as the Navajo Nation.[1] Mining of U ore deposits in the region occurred between 1940 and 1980 but left a profound impact on the environment because

[a] *Department of Civil and Environmental Engineering, University of Iowa, 4105 Seamans Center for the Engineering Arts and Sciences, Iowa City, IA 52242, USA. E-mail: david-cwiertny@uiowa.edu; Tel: +(319) 335 1401*
[b] *Department of Civil, Construction & Environmental Engineering, University of New Mexico, Albuquerque, NM 87131, USA*
[c] *Department of Chemical and Biochemical Engineering, University of Iowa, 4133 Seamans Center for the Engineering Arts and Sciences, Iowa City, IA 52242, USA*
[d] *Department of Chemistry, University of Iowa, Iowa City, IA 52242, USA. E-mail: tori-forbes@uiowa.edu; Tel: +(319) 384 1320*
[e] *Center for Health Effects of Environmental Contamination, The University of Iowa, 251 North Capitol Street, Chemistry Building - Room W195, Iowa City, Iowa 52242, USA*
† Electronic supplementary information (ESI) available: ESI includes additional methodological details associated with fabrication of functionalized nanofibers and U^{6+} analysis, as well as additional results related to the characterization and performance of functionalized nanofibers. See DOI: 10.1039/c9ew00834a

of the presence of thousands of abandoned and open mines.[2,3] Over 500 abandoned mines containing residual U within waste rock are located on Navajo lands and contribute to U concentrations in unregulated water sources that exceed the U.S. Environmental Protection Agency Maximum Contaminant Level (US EPA MCL) of 30 μg L^{-1}.[4–7] In surface waters and shallow aquifers, U is in the hexavalent state and forms the uranyl (UO_2^{2+}) cation, which can further complex to ligands to form soluble species.[8] Source waters in the region range from alkaline to circumneutral pH and are high in dissolved carbonate, leading to the formation of soluble uranyl complexes that can contribute to high concentrations of total U in drinking water sources.[5,9,10] Some waters near mine waste sites can have pH values lower than 4 due to acid mine drainage.[11]

For resource-constrained communities without reliable access to centralized water treatment systems, point-of-use (POU) and point-of-entry (POE) technologies are an attractive option for improving drinking water quality. For example, existing US EPA-approved small system compliance technologies (SSCT) for POU treatment of U^{6+} include ion exchange (IX) and reverse osmosis (RO) technologies, while activated alumina can also remove U^{6+} but is not listed as an SSCT.[12] Although all of these approaches are capable of removing total U to levels below the US EPA MCL, these technologies can be difficult to use and maintain in underserved populations. For example, RO can involve high capital costs, requires high operating pressures with associated energy demand, and produces a concentrated waste brine that would need proper disposal.[13] In places relying on unregulated water sources,[14] as is the case in some locations within the Navajo Nation,[15] such advanced technologies would be of limited value.

We have previously demonstrated the use of electrospinning to produce novel, chemically reactive membranes for simultaneous filtration of suspended particles and sequestration or destruction of dissolved chemical contaminants.[16–19] For materials targeting dissolved metals, we have used surface-segregating surfactants, especially those with quaternary ammonium groups, to produce surface-functionalized polymeric nanofibers that effectively function as ion exchange materials. More recently, we have also used post-fabrication routes to introduce specific binding moieties on the nanofiber surface. For U^{6+}, a popular moiety is amidoxime (AO),[20,21] which is highly specific for the uranyl cation and can be produced *via* reduction of polyacrylonitrile (PAN),[22] a polymer commonly used in electrospinning, with hydroxylamine (Table 1). Indeed, we have previously amidoximated PAN (AO-PAN) nanofibers for the selective concentration of U^{6+} to improve environmental sensing *via* surface enhanced Raman spectroscopy (SERS).[23] However, we have not yet explored this material more generally for water treatment applications, where timescales of uptake, material capacity, performance across pH, and response to common co-solutes (*e.g.*, alkalinity and hardness typical of U-contaminated waters) will likely influence performance.

Here, we fabricate various functionalized PAN nanofibers using electrospinning and explore their applications for the removal of U^{6+} from contaminated water supplies. To introduce U^{6+}-specific binding sites, we not only used post-synthesis amidoximation of PAN nanofibers, but we also developed synthesis recipes integrating various N- and P-containing surfactants to produce functionalized nanofibers (Table 1). For N-containing surfactants, we focused on those with quaternary ammonium groups (*e.g.*, tetrabutyl ammonium bromide or TBAB and Aliquat® 336)[24,25] because these are analogous to strong base anion exchange sites and thus would be expected to electrostatically bind negatively charged U^{6+} complexes typical of circumneutral pH.

Table 1 (a) N-containing (quaternary ammonium) and (b) P-containing binding agents, as well as (c) the amidoximation reaction of PAN, used for U capture herein

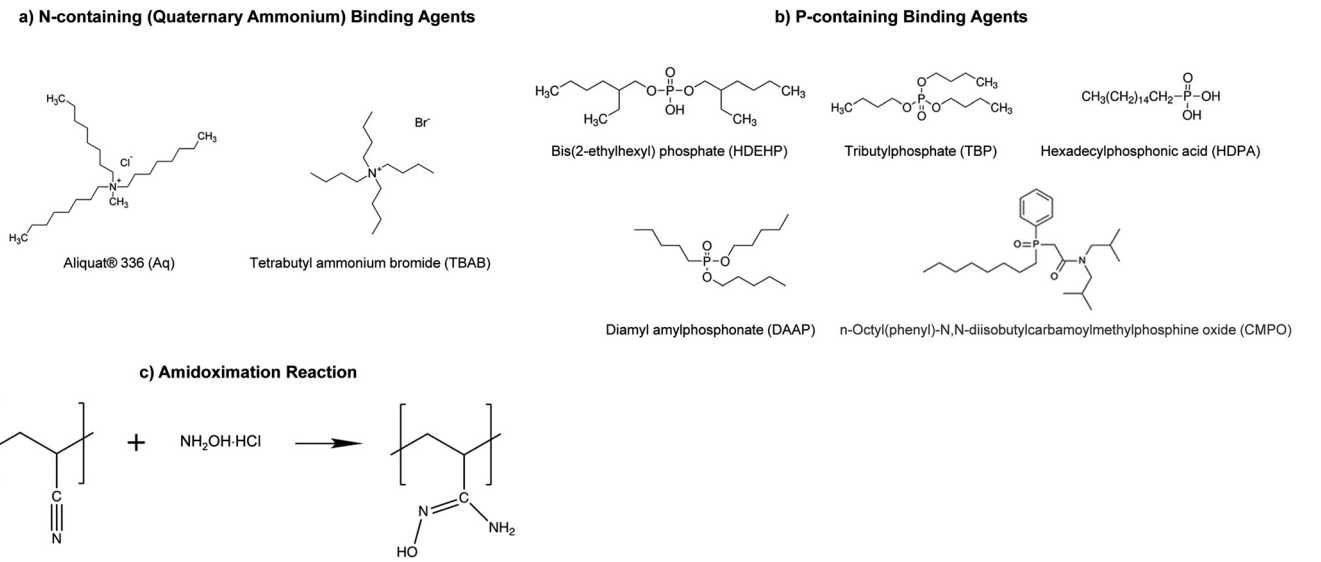

P-containing binding agents included surfactants with phosphoric or phosphonic acid groups [*e.g.*, di-(2-ethylhexyl)-phosphoric acid (HDEHP) and heptadecylphosphonic acid (HDPA)][26–28] that form strong complexes with U^{6+} and may ultimately promote more extensive removal *via* surface precipitation. We also explored the integration of commercially available P-based extractants [diamyl amyl phosphonate (DAAP)], *n*-octyl(phenyl)-*N*,*N*-diisobutylcarbamoylmethylphosphine oxide (CMPO), and tributyl phosphate (TBP) that are commonly marketed (*e.g.*, Eichrom's TRU Resin with CMPO)[29] to separate U^{6+} from complex media in nuclear waste streams. For example, phosphate esters such as TBP have been used extensively in the nuclear fuel cycle to selectively extract UO_2^{2+} cations from fission products and transuranics in liquid–liquid processes; although the exact nature of this extraction is not fully delineated it is suggested to proceed *via* outer sphere complexes, particularly with uranyl nitrate species.[30,31]

After nanofiber synthesis and characterization of their physical and chemical properties, we tested eight different functionalized materials for U^{6+} uptake to identify the most promising candidates for further material development. The performance of the most promising materials for U^{6+} capture was then explored across a range of pH, dissolved U^{6+} concentrations, and water chemistries, including in a dead-end, flow through filtration system typical of low-pressure POU water treatment. Outcomes of this work help to establish the viability of functionalized nanofiber filters as low pressure water treatment technologies for use in areas afflicted by U^{6+} contamination of limited freshwater resources.

Materials and methods

Reagents

A complete list of reagents can be found in the ESI.† Nanofibers of PAN (MW 150 000, Aldrich) were fabricated by electrospinning on a support layer of polyvinylidene difluoride (PVDF; MW 180 000, Aldrich). Binding agents (Table 1) included N-containing tetrabutylammonium bromide (TBAB; Sigma Aldrich) and Aliquat® 336 (Aq; Alfa Aesar) and P-based binding agents tributyl phosphate (TBP; Sigma Aldrich), diamyl amylphosphonate (DAAP; Sigma Aldrich), CMPO (Carbosynth; 98%), bis(2-ethylhexyl) phosphate (HDEHP; 97%, Aldrich), and hexadecyl phosphonic acid (HDPA; 97%, Aldrich). Amidoximation of PAN used hydroxylamine hydrochloride (98%, Aldrich) and sodium hydroxide (97.0%, Fisher Scientific).

Electrospinning

Full details of nanofiber synthesis are provided in the ESI.† Nanofiber mats were synthesized on a custom-built electrospinning rig described in our previous work.[16–18] PAN nanofibers were deposited on a layer of PVDF nanofibers to enhance the mechanical stability of the materials; PVDF was electrospun first, and after completion of the PVDF layer, a layer of PAN was subsequently deposited *via* sequential electrospinning. The resulting bilayer material contained 50 wt% PAN and 50 wt% PVDF. For production of AO-PAN, the two-layer polymer structure was reacted with hydroxylamine according to the amidoximation procedure described in the ESI,† which was adapted from our earlier work.[23]

Mats with surfactant-based binding agents followed the same synthesis procedure but used PAN sol gel precursor solutions containing the desired binding agent. Most surfactant-functionalized mats were prepared using a precursor solution with 7 wt% PAN and up to 3 wt% of binding agent dissolved in DMF (all wt% are reported relative to the total weight of sol gel). Because HDPA exhibited limited soluble in DMF, mats containing HDPA were only prepared with 6 wt% PAN and either 0.5 or 1 wt% HDPA dissolved in DMSO. All solutions were then stirred at 60 °C for 2 h at 700 RPM to ensure complete dissolution of the surfactants and a homogenous precursor solution.

Nanofiber characterization

Nanofiber morphology and diameter were determined through imaging with scanning electron microscopy (SEM; S-4800, Hitachi). Fourier transform infrared spectroscopy (FTIR; Nicolet™ iS™ 50 FTIR Spectrometer) was used to examine all functionalized nanofiber formulations to confirm the presence of PAN and the binding agent. Mat pore volume and specific surface area were determined by N_2-BET adsorption isotherms on a Quantachrome NOVA 4200e Analyzer. X-ray photoelectron spectroscopy (XPS) was performed using a Kratos Axis Ultra spectrometer to characterize the near surface region (~top 5–10 nm) of the functionalized nanofibers before and after U^{6+} uptake experiments. Additional materials characterization details can be found in the ESI.†

Uranium uptake experiments

Initial comparison of different binding agents. To identify the most promising binding agents, uptake experiments with functionalized nanofibers were conducted with 10 μM total U^{6+} at either pH 2 (Milli-Q Ultrapure water adjusted with 5 N HNO_3) or pH 6.8 (10 mM HEPES, which is commonly used in environmental and biological systems, including our prior work with U^{6+} uptake and sensing on AO-PAN).[23] These pH values were chosen for their relevance to U^{6+} treatment systems, simulating remediation of U-contaminated acid mine drainage (pH 2) and treatment of U-contaminated drinking water sources (pH 6.8). Solutions of U^{6+} were prepared by diluting a 1000 mg L^{-1} depleted uranium nitrate (SPEX CertiPrep) stock to the desired initial concentration, typically 1 or 10 μM (0.24 or 2.4 ppm, or mg L^{-1}, as U^{6+}, respectively), in a 50 mL plastic conical vial. To initiate an uptake study, a functionalized PAN mat was added to a conical vial at a mass loading of 0.25 g L^{-1} (~0.25 cm^2 L^{-1}) and then incubated while mixing. Rate experiments confirmed that uptake of U was relatively rapid in all systems (see Fig. S1†), with most uptake achieved in the initial 2 h. Because a small amount of U^{6+} uptake continued over longer timescales in some

systems, all sorption studies were allowed to proceed for 16 h, at which point there was no significant change in solution concentration over time for any system (*i.e.*, equilibrium). In all instances, minimal pH drift was observed (<0.1 pH units) during the 16 hour reaction period, after which mats were removed from the solution and analyzed for their sorbed U^{6+} content as described below.

pH edge and isotherm experiments. For the most promising materials identified from initial uptake studies, more in depth pH edge and isotherm experiments were conducted using experimental systems identical to those described above. For pH edge experiments, systems were assembled at initial pH values between 2 and 7. To avoid any influence of different buffers at different pH values, all experiments were conducted in Milli-Q Ultrapure water that was adjusted to the desired pH with either 5 M NaOH or HNO_3. pH edge experiments were conducted at initial U^{6+} concentrations of both 1 and 10 μM, and all systems were allowed to react for 16 hours to achieve equilibrium. At the conclusion of the experiment, the final pH value of each reactor was recorded to measure pH drift during incubation, which was typically <0.5 pH units.

For sorption isotherms, initial U^{6+} solutions were prepared at concentrations of 0.1, 0.5, 1, 5 and 10 μM U. Sorption isotherms were conducted at either pH 2 (Milli-Q Ultrapure water adjusted with either 5 N NaOH or 5 N HNO_3) or pH 6.8 (10 mM HEPES). All other experimental conditions are as described previously for pH edge systems (*e.g.*, 16 h incubation period).

Simulated POU filtration. The performance of optimal nanofiber mat formulations was evaluated in a dead-end, flow-through filtration system (Fig. S2†) to simulate their application in water treatment. The filter holder (Cole-Parmer) had a 25 mm outer diameter with an active filtration area of 3 cm^2. Mats were cut to fit within this holder and typically weighed between 10–13 mg per layer of mat (depending on the formulation). To increase the mass of nanofibers used for treatment, thicker filters were created by stacking multiple layers of material with the same effective filtration area, thereby increasing the residence time for U-containing influent within the nanofiber mat. Flow-through conditions were created using influent flowrates of 0.4 or 0.8 mL min^{-1} driven by a 60 mL syringe loaded on a syringe pump (New Era Pump Systems, Inc.). These flowrates produce fluxes ranging from 80 to 160 LMH (0.4 to 0.8 mL min^{-1} assuming 3 cm^2 active area), which correspond to the high range for ultrafiltration (80 LMH) and low end of microfiltration (160 LMH).[32] Filters were preconditioned with 20 mL of a 10 mM HEPES solution (pH 6.8) followed by either 120 or 240 mL of a 1 μM U^{6+} (0.24 ppm) solution in 10 mM HEPES at pH 6.8. Additional tests were conducted using solutions with 500 mg L^{-1} Ca^{2+} and 500 mg L^{-1} HCO_3^- to evaluate the influence of environmentally relevant ions. Effluent was collected in 4 mL samples for every 10 mL of filtered solution for analysis of dissolved U by ICP-MS as described below.

Analytical methods

For batch uptake systems, U analysis was conducted *via* liquid scintillation counting (LSC) using a ^{232}U radiotracer (NIST traceable standard, Eckert & Ziegler) with a 3.5 Bq spike per 20 mL of solution. The activity of solutions was measured by adding 2 mL aliquots from each reactor to 10 mL of EcoLite scintillation cocktail (MP Biomedicals) in a 20 mL scintillation vial. Sorbed uranium was measured by removing the mat from the reactor and placing it into a 20 mL scintillation vial with 10 mL of Ecolite scintillation cocktail. Vials were shaken and left overnight to dark adapt (energy in scintillation cocktail from light is able to leave) and provide ample time for the polymer mats to dissolve in the scintillation cocktail. Samples were then counted on a liquid scintillation counter (LSC; Packard 1600CA Tri-Carb liquid scintillation analyzer) for 40 minutes. The range of 100 and 2000 keV was used to exclude beta signals produced by daughter isotopes of ^{238}U, ^{234}Th and ^{234}Pa. Generally, in samples collected from equilibrated experimental systems, LSC analysis of both solution phase and sorbed uranium indicated complete mass balance.

ICP-MS analysis was used to analyze the effluent for U^{6+} collected from the flow through systems. Effluent samples analyzed by ICP-MS analysis were acidified with 2% HNO_3 (trace metals grade, Aldrich) and filtered with 0.45 μm filters prior to analysis on an Agilent Technologies 7900 ICP-MS. Argon was used as the carrier gas in low matrix mode and no collision gas was used. Mass-to-charge ratios of 7, 89, and 205 were used for tuning of the instrument prior to running calibration standards and samples in triplicate. ^{209}Bi (Inorganic Ventures) was used as the internal standard at a concentration of 10 ppb. We note, initial studies indicated that trace amounts of some surfactants likely leached from the functionalized mats during uptake experiments, and this dissolved surfactant residual present in samples interfered with ICP-MS analysis. To avoid this interference, all surfactant-functionalized materials were washed with DI water prior to use in uptake experiments where samples required ICP-MS analysis (*e.g.*, flow through systems). The washing procedure involved placing 5 mg of a functionalized PAN mat in a 50 mL conical vial with 10 mL of Milli-Q Ultrapure water. Vials were mixed end over end for 24 hours, while three changes of the water were performed over that time interval.

Results and discussion

Comparison of functionalized PAN Nanofibers for U^{6+} uptake

Initial uptake studies explored the performance of PAN nanofibers functionalized with different P- and N-containing binding agents as a function of their wt% in PAN at pH 2 and pH 6.8 (Fig. 1). Of the P-functionalized materials, integration of HDEHP (at pH 2) and HDPA (at pH 2 and 6.8) resulted in the greatest uptake (between 35–55% uptake for 0.25 g L^{-1} of nanofibers and initially 10 μM U^{6+}), with U^{6+} binding on other P-containing materials (*e.g.*, TBP, CMPO,

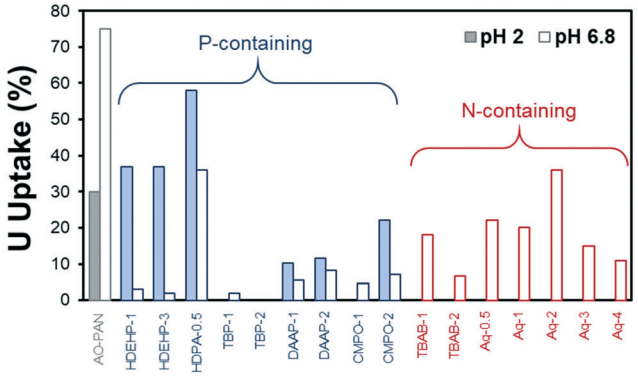

Fig. 1 Performance comparison of functionalized PAN nanofibers for U^{6+} uptake at pH 2 (solid bars) and pH 6.8 (open bars). Uptake data are shown for different binding agents (with wt% in sol gel indicated) after 16 h of equilibration between an initial concentration of 10 μM U^{6+} and 0.25 g L^{-1} of each mat. Experiments were conducted in 10 mM HEPES at pH 6.8 and water acidified to pH 2 with HNO_3.

and DAAP) being very limited (~10%) or negligible at both pH values. Performance of HDEHP was effectively invariant over the concentrations in PAN we explored (1 and 3 wt%); thus, all additional work with HDEHP was conducted at 1 wt% to minimize the amount of reagent needed for synthesis. For HDPA-containing materials, optimal performance was observed at a concentration of 0.5 wt% in PAN.

For N-containing binding agents, U^{6+} uptake was only observed at pH 6.8, with no detectable binding at pH 2. Generally, Aq-containing materials outperformed those with TBAB. Although comparable uptake of U was observed for 1 wt% in PAN of either Aq or TBAB, increasing the concentration to 2 wt% resulted in higher uptake with Aq but lower uptake for TBAB-containing materials. We have previously found that the mass ratio of quaternary ammonium surfactant to polymer can influence the performance of the functionalized PAN.[17] Accordingly, additional studies exploring the influence of Aq concentration between 0.5 to 4 wt% were conducted, revealing maximum U^{6+} uptake at 2 wt% in PAN. All additional uptake studies were conducted at this optimal Aq loading.

AO-PAN exhibited the greatest uptake at pH 6.8, nearly double of the removal displayed by either HDPA- or Aq-containing materials at the same pH value. At pH 2, AO-PAN also produced measurable uptake of U^{6+} at a level comparable to that observed for HDEHP-containing materials but below the extent of removal achieved with HDPA-functionalized PAN.

We note that beyond basic characterization to ensure all materials tested in Fig. 1 were comparable in morphology (*i.e.*, nanofibers), no additional investigations were performed to better understand differences in the performance of P- and N-containing binding agents. Several possibilities exist, including differences in the chemistry of the binding sites available on the functionalized PAN (*e.g.*, the relative affinity for U^{6+} uptake on different P-containing functionalities). We also cannot rule out differences in the location of the binding sites in the fibers after electrospinning, as some binding agents may surface segregate to a greater extent than others. Thus, it is certainly possible that the performance of materials with low U^{6+} uptake in Fig. 1 could be further optimized, but such work is beyond the scope of the current study.

Characterization of optimally performing nanofibers

Key characterization details for optimal nanofiber formulations including AO-PAN and those containing either 2 wt% Aq, 0.5 wt% HDPA, or 1 wt% HDEHP are summarized in Fig. 2. Overall, there were only a few notable differences between the functionalized PAN nanofibers explored for U uptake. The average diameter for all functionalized PAN nanofibers was between 110–160 nm, but the typical standard deviation from the nanofiber distribution (see histograms in Fig. S3†) indicates all diameters are statistically equivalent. Moreover, there was no obvious influence of increasing functionalization, either based on wt% of embedded P- or N-containing binding agents or amidoximation, on the average or distribution of nanofiber diameters. Similarly, the specific surface area for all materials fell between 11 and 21 $m^2\ g^{-1}$ (with most being statistically equivalent based on the standard deviation from replicate analyses), with no clear trends in surface area based upon the amount or type of integrated binding sites. There were some modest differences in the pore volume of different materials, especially for HDEHP-containing nanofibers that exhibited pore volumes [13 (±5) × 10^{-3} $cm^3\ g^{-1}$] considerably lower than the other materials [for example, 45 (±5) × 10^{-3} $cm^3\ g^{-1}$ for PAN]. We speculate this could be an indication that HDEHP preferentially locates within the pore structure of PAN, blocking pore access. Analysis *via* FTIR (Fig. S4†) was consistent with expectations for PAN-based polymers, but typically revealed little evidence of the different functionalization routes we employed except for HDEHP and amidoximation. This is not necessarily surprising because FTIR is a bulk characterization technique and most binding agents were present at a relatively low wt% in the functionalized nanofibers.

pH-Dependent U uptake

At an initial U^{6+} concentration of 10 μM, PAN with 0.5 wt% HDPA exhibited among the highest uptake (>60% of total U^{6+}) over the entire pH range (Fig. 3a). AO-PAN achieved its lowest removal at pH 2 (~40%), but U^{6+} removal increased with pH, producing relatively high and constant removal between pH 3 and 7 (~80%). PAN with 1 wt% HDEHP exhibited the opposite behavior relative to AO-PAN; its highest uptake was at pH 2 (~50%), but U^{6+} removal decreased markedly at pH 3 (<20%) and was maintained at this low level for all higher pH values explored. Finally, PAN with 2 wt% Aq exhibited the lowest removal overall (between 0–15%), but U^{6+} uptake did modestly increase with increasing pH values.

Notably, at a lower initial U^{6+} concentration of 1 μM (Fig. 3b), different pH-dependent removal trends were observed for some, but not all, materials. While trends in U^{6+}

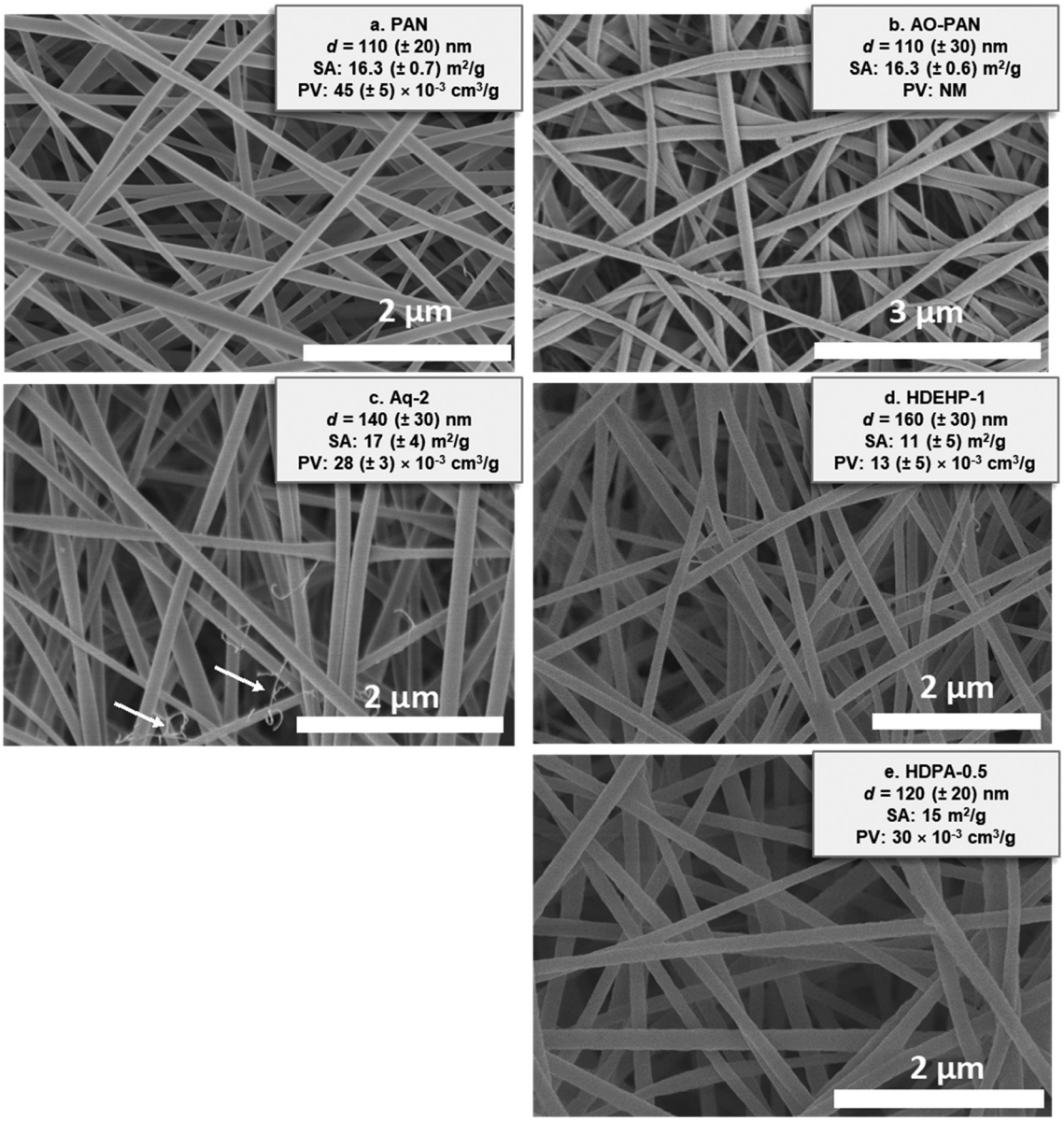

Fig. 2 Representative SEM images of synthesized nanofibers, where the numbers in the material name correspond to the wt% of the integrated surfactant (where appropriate). Also provided are results from N_2-BET measurements of specific surface area (SA in $m^2\ g^{-1}$) and pore volume (PV in $cm^3\ g^{-1}$). Average and standard deviations are provided from duplicate measurements, where available. NM means "Not Measured", as there was insufficient amount of material fabricated to allow for SA or PV analysis. For some surfactant-functionalized materials (*e.g.*, Aq), small amounts of "hair-like" structures were observed (see white arrows) but were not present in sufficient abundance to alter nanofiber diameter distributions.

uptake at 1 μM were comparable to those observed at higher initial U^{6+} for HDEHP- and Aq-containing PAN, AO-PAN and HDPA-containing PAN exhibited different pH-dependent performance. For AO-PAN, this difference was only observed at higher pH values (pH $>$ 5). Specifically, whereas removal was relatively constant (~80%) above pH 5 in 10 μM U^{6+} systems, uptake decreased steadily from pH 5 (~80%) to pH 7 (~40%) in 1 μM U^{6+} systems. A much greater difference in performance between low and high concentration U^{6+} systems was observed with HDPA-functionalized PAN. While removal at 10 μM U^{6+} was greater than 60% across all pH values, the removal in 1 μM U^{6+} systems was greatest at pH 2 (~50% U^{6+}) and decreased steadily until pH 4 (~10%), above which uptake was minimal.

A possible explanation for the difference in performance between 1 μM and 10 μM U^{6+} systems for AO-PAN and HDPA-containing materials could be removal *via* surface precipitation at high initial U^{6+} concentrations, similar to processes previously reported to occur on mineral phases[33] and functionalized polymers.[34] For AO-PAN, for example, the exact binding mechanism for uranium to amidoxime is still widely disputed, with arguments for either monodentate (binding with either N or O) or bidentate (binding to both N and O) complexes in prior investigations.[35] Pekel *et al.*[36] suggested

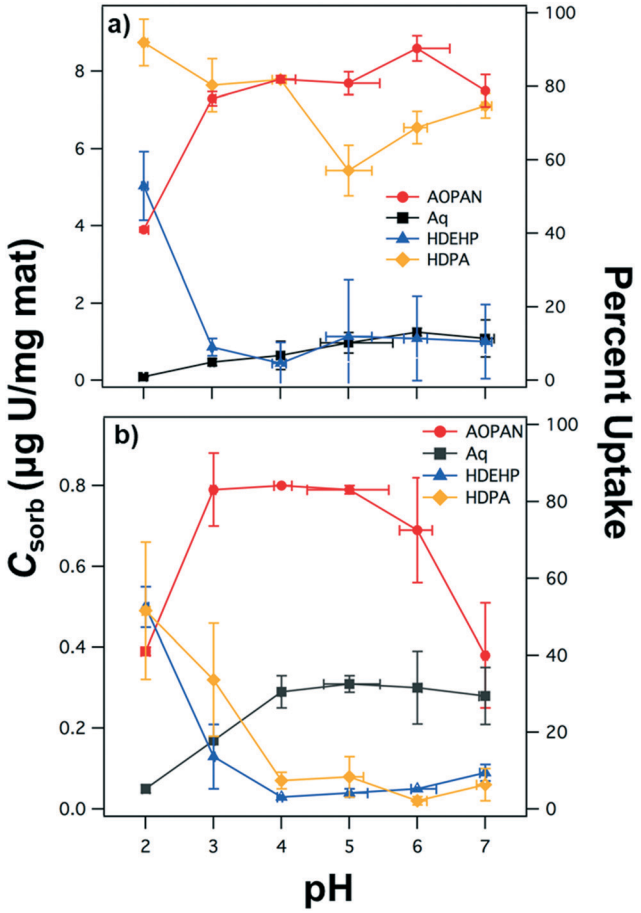

Fig. 3 Sorbed U^{6+} concentration as a function of solution pH at an initial U^{6+} concentration of (a) 10 µM and (b) 1 µM for AO-PAN and PAN with either 2 wt% Aq, 0.5 wt% HDPA, or 1 wt% HDEHP. All materials were tested in water (pH adjusted with 5 M NaOH or HNO_3) without buffer. Vertical error bars reflect standard deviation of duplicate trials while horizontal error bars represent the range of pH drift observed over the course of the experiment (~16 h). A nanofiber mass loading of 0.25 g L^{-1} was used in all experiments.

that deprotonation of the imine group was important for chelation to uranyl by exchange of H^+ with UO_2^{2+} while Hirotsu *et al.*[37] reported that ligand exchange (and ion exchange of H^+ depending on pH) occurs during uranyl uptake. In both 1 and 10 µM U systems at pH 2, similar uranium removal occurs (~40%) with 100% of the uranyl species being UO_2^{2+}, suggesting that the high H^+ concentration competes with UO_2^{2+} in the amidoxime group. A decrease in the H^+ concentration (*i.e.*, increasing pH between 3 and 5) results in much greater (~80%) U^{6+} removal. Hydrolysis of UO_2^{2+} starts at pH 4, and it is no longer the dominant species by pH 5 (see Guillaumont *et al.*[38] and speciation diagrams for 1 and 10 µM U^{6+} solutions in Fig. S5†). In 10 µM systems, speciation diagrams suggest that insoluble $UO_2(OH)_2{\cdot}H_2O$ is the dominant species by pH ~ 5.5, and we suspect this species may be precipitating on the surface based upon the high (~80%) removal still observed at pH 6 and 7 in 10 µM U^{6+} systems. In contrast, the decrease in removal with increasing pH observed in 1 µM U^{6+} systems (~70% at pH 6 and ~40% at pH 7) may be indicative of speciation changes that occur above pH 5; we expect UO_2OH^+ to be the dominant form at pH 5 and 6 (~50% and ~40% of total U^{6+}, respectively) followed by $UO_2(OH)_2{\cdot}H_2O$ at pH 7 (~90% of total U). Because ligand exchange is expected to occur in these regions, the lower uptake may also be due to slower kinetics involved with ligand exchange.[39]

For HDPA-functionalized PAN, uranyl phosphate complexes are known to have very low logK_{sp} values (−49.00 to −53.33)[40] compared to that of hexavalent uranyl hydroxides (−21.75 to −24.10)[41] and uranyl carbonates (−13.29 to −14.91),[40] which enables uranium phosphates to precipitate in even acidic solutions. This behavior has been seen before with phosphate-functionalized TiO_2, where an insoluble sodium autunite ($NaUO_2PO_4$) complex formed after uranium sorption in acidic solutions (pH 2).[42] In this earlier work, the mechanism of uptake was described as a combination of adsorption and surface complexation that shifts to surface precipitation;[42] such a scenario may also be likely for U^{6+} removal on HDPA-functionalized nanofibers in our 10 µM U^{6+} systems, whereas only adsorption and surface complexation occur in our 1 µM U^{6+} systems.

For HDEHP- and Aq-containing nanofibers, trends in pH-dependent removal lend insight into their mechanism of U^{6+} binding. For example, the sorption capacity of HDEHP-containing materials is reduced considerably above pH 3. HDEHP has a pK_a of 1.47,[43] and thus will become increasingly more deprotonated (*i.e.*, more anionic) from pH 2 to pH 3. Over this same pH range, U^{6+} removal decreases from 50% to ~10% in both 1 and 10 µM systems. Thus, U^{6+} removal does not appear to proceed *via* a purely electrostatic mechanism (*i.e.*, positively charged UO_2^{2+} bound by negatively charged HDEHP sites), suggesting that U^{6+} uptake may also occur by exchange of H^+ during uranyl coordination, which has been previously observed by Kiwan and Amin.[44] Moreover, hydrolysis of the UO_2^{2+} cation should not affect U^{6+} uptake with HDEHP because hydrolysis products are not abundant until pH 4 for solutions containing 1 or 10 µM U^{6+} (see Guillaumont *et al.*[38] and Fig. S5†). As a final consideration, the chemical differences between HDEHP and HDPA may also lend insight regarding the mechanism of U^{6+} uptake. HDEHP contains only one hydroxyl group available for U^{6+} binding, whereas HDPA has multiple hydroxyls that may allow it to chelate and precipitate U^{6+} in a manner similar to the phosphate anion.

At both initial concentrations (1 and 10 µM), Aq-containing nanofibers produced a slight increase in U^{6+} uptake with increasing pH. This behavior likely reflects that uptake of U^{6+} by Aq is dependent on the fraction of anionic uranyl species present in solution. Aq is positively charged across the pH range investigated, and as a strong base ion exchanger, it has been shown to bind negatively charged uranium complexes.[45–47] We therefore hypothesize that anion exchange is the main mechanism for uptake of U^{6+} on Aq-functionalized nanofibers, but further verification of this mechanism is warranted. In fact, for pure aqueous systems,

anionic uranyl species (*e.g.* $UO_2(OH)_3^-$) should not be formed until ~ pH 7 (see Guillaumont *et al.*[38] and Fig. S5†). Furthermore, while negatively charged species can form in the presence of carbonate [*e.g.*, $(UO_2)_2CO_3(OH)_3^-$ can form as early as pH 4], these anionic carbonate species are only produced at dissolved CO_2 concentrations higher than those in our experimental systems.[48]

Sorption isotherms for U on functionalized PAN nanofibers

To explore their capacity for U^{6+} uptake, sorption isotherms were collected with AO-PAN and PAN containing either 2 wt% Aq, 0.5 wt% HDPA, or 1 wt% HDEHP (Fig. 4). Functionalized PAN nanofibers were tested over a range of U^{6+} concentrations that varied from just below its MCL in drinking water (~0.1 μM) to the more extreme levels of U^{6+} contamination that may be present in some affected water resources (10 μM). We only developed isotherms at the optimal pH value observed for each functionalized material in pHedge experiments. PAN nanofibers functionalized with HDPA and HDEHP were tested in acidic conditions (pH 2), whereas isotherms for Aq-containing PAN and AO-PAN were conducted at pH 6.8.

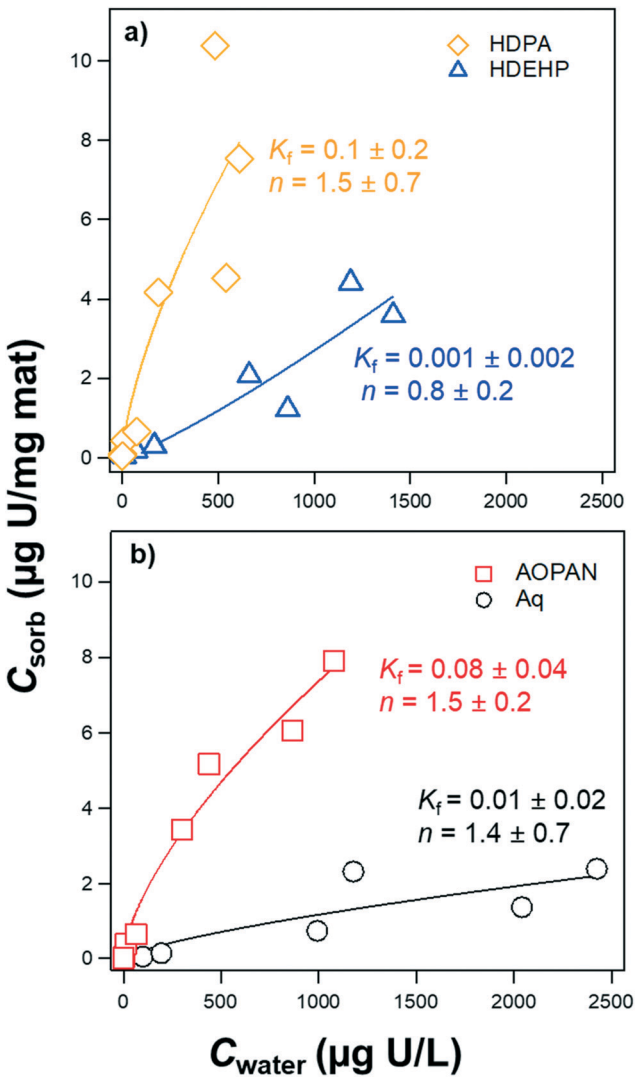

Fig. 4 Sorbed U^{6+} concentration as a function of solution phase U^{6+} concentration at equilibrium for AO-PAN and PAN with either 2 wt% Aq, 0.5 wt% HDPA, or 1 wt% HDEHP. Sorption isotherms were conducted in either (a) water acidified to pH 2 with HNO_3 for HDPA- and HDEHP-containing PAN or (b) 10 mM HEPES at pH 6.8 for Aq-containing and AO-functionalized PAN. Freundlich equation fits with model fit parameters are shown. Data are shown from duplicate isotherm experiments conducted on separate days with each material.

Overall, a trend of increasing solution phase U^{6+} concentration resulted in increased sorbed U^{6+} concentrations for all materials, and the extent of uptake generally agreed well with our other experimental results (see Fig. 1 and 3). To model U^{6+} uptake, we used the empirical Freundlich isotherm model [$C_{sorbed} = K_f(C_{aq})^{1/n}$, where K_f is the Freundlich isotherm parameter and n is the degree of linearity] because we observed no clear evidence consistent with surface site saturation (as would be expected for a Langmuir-type isotherm). The parameters for the Freundlich isotherms determined by non-linear regression analysis are summarized in Fig. 4 for each functionalized material. At pH 6.8, AO-PAN far exceeded the uptake of Aq-containing mats, and uptake on AO-PAN was clearly non-linear (n = 1.5 ± 0.2). At pH 2, U^{6+} sorption on HDPA-functionalized PAN (n = 1.5 ± 0.7) was considerably greater than HDEHP-containing materials (n = 0.8 ± 0.2), with model outputs indicating that sorption isotherms did not significantly differ from linearity over the range of U^{6+} concentrations explored (although relatively large standard deviations in model fits were observed because of the modest degree of variability in uptake observed between two replicate isotherm experiments).

Even when uptake was clearly non-linear (*e.g.*, AO-PAN), we did not achieve the sorption capacity of any materials using these isotherm conditions. At the highest initial U^{6+} concentration explored of 10 μM (or 2.4 mg L^{-1}), corresponding concentrations for sorbed U^{6+} were approximately 4 and 10 μg mg^{-1} at pH 2 for HDEHP- and HDPA-containing nanofibers, respectively, and approximately 2 and 8 μg mg^{-1} at pH 6.8 for Aq-containing and AO-PAN nanofibers, respectively. A prior investigation of AO-PAN nanofibers with a polystyrene core shell reported a maximum sorbed concentration of 130 μg mg^{-1} (conditions: 1 g mat L^{-1}; initial uranium concentration of 100 mg L^{-1}; pH 4).[49] Phosphate-functionalized polyethylene had a maximum sorbed concentration of 180 μg mg^{-1} (conditions: 0.2 g mat L^{-1}; initial uranium concentration of 50 mg L^{-1}; pH 8.2).[50] Strong base anion exchangers, similar to Aq, have not been used for U^{6+} uptake in nanofibers but show high uptake in resins at ~50 μg mg^{-1} in groundwater (conditions: initial U^{6+} concentration of 1200 μg L^{-1}; pH 6.5; flow through system).[45] Although many of these prior investigations report sorbed U^{6+} concentrations that are greater than what we report for the functionalized nanofibers herein, we note that several of these earlier works used initial U^{6+} levels far exceeding the concentrations used in our experimental systems. Thus, we cannot rule out that some of these

high levels of U^{6+} uptake may reflect U^{6+} removal *via* surface precipitation, as we suspect may occur at high U^{6+} and high pH on AO-PAN and HDPA-functionalized PAN, leading to greater removal *via* multi-layer growth of a separate U-containing solid phase.

To probe the nature of surface bound U^{6+}, XPS analyses were collected for all functionalized materials after U^{6+} uptake experiments conducted with an initial concentration of 10 μM. XPS analysis of these reacted nanofiber mats detected the presence of U^{6+} on the surface of all functionalized materials (Table S1†). High resolution U 4f spectra (Fig. S6†) contained signals corresponding to the U $4f_{7/2}$ and U $4f_{5/2}$ doublet on HDPA-, HDEHP-, Aq- and AO-PAN functionalized materials. However, while confirming the presence of U^{6+} on the surface of all functionalized nanofibers, XPS analysis was unable to provide any greater details regarding the nature of U^{6+} surface species or complexes.

Simulated treatment in flow through systems

Break through curves showing normalized U^{6+} concentration (*i.e.*, effluent concentration normalized to influent concentration; $C_{effluent}/C_{influent}$) as a function of volume of water treated from dead-end filtration flow through systems are shown in Fig. 5 for AO-PAN and HDPA-containing nanofiber filters at pH 6.8. For such curves, we define filter exhaustion or complete breakthrough as when the effluent U^{6+} concentration is equal to that of the influent concentration ($C_{effluent} = C_{influent}$), which would mean either that the materials are saturated (*i.e.*, all binding sites are occupied and thus not capable of removing any more uranium) or that timescales for U^{6+} uptake on the remaining available binding sites are far slower than the residence time for U^{6+} in the nanofiber filter system. With an influent concentration of 1 μM U^{6+} (240 μg L^{-1}) at pH 6.8, we note that any normalized concentration above ~0.1 would be considered above the MCL for uranium (30 μg L^{-1}).

For AO-PAN (Fig. 5a), the lowest filter mass tested (13 mg) did not show complete breakthrough, but produced approximately constant, incomplete (~40%) removal of U^{6+} where $C_{effluent}$ was ~60% of $C_{influent}$. Increasing the mass of AO-PAN (from 13 mg to 26 mg by adding a second filter layer) resulted in effectively complete removal of U^{6+}. Based on these results, U^{6+} uptake on AO-PAN filters appears kinetically limited under our experimental conditions. At lower filter mass (13 mg), breakthrough was approximately steady state; complete saturation of the filter did not occur (*i.e.*, there was always some residual capacity for U^{6+} removal), but U^{6+} was present in the effluent and the effluent concentration was not changing over time. Addition of more filter mass (from 13 mg to 26 mg) increased the contact time between the U^{6+}-containing solution and the AO-PAN filter, which in turn resulted in near-complete removal of U over the duration of the 120 mL filtration experiment. Notably, at the conclusion of the experiment with the 26 mg filter, the mass of U^{6+} captured was ~1.1 μg mg^{-1} after treating 120 mL of water, which is well below the maximum sorbed concentration of ~8 μg mg^{-1} observed in batch isotherm experiments with AO-PAN (see Fig. 3). This suggests that AO-PAN materials still have considerably more sites available for U^{6+} binding. A second run of a 26 mg filter over 240 mL of 1 μM U^{6+} influent revealed removal of all influent uranium to levels that were below detection in the effluent and thus below the EPA MCL (Fig. S7;† all $C_{effluent}$ values were below detection or 1 μg L^{-1} *via* our ICP-MS analytical method). Once again, this sample still had not reached saturation and the amount of U^{6+} bound on the reacted AO-PAN filter (~2.2 μg mg^{-1}) was only ~25% of the max U^{6+} sorption found in batch. Once again, this supports kinetically limited U^{6+} removal in AO-PAN systems, where thicker filter materials or lower flow rates will produce higher residence times and better removal performance.

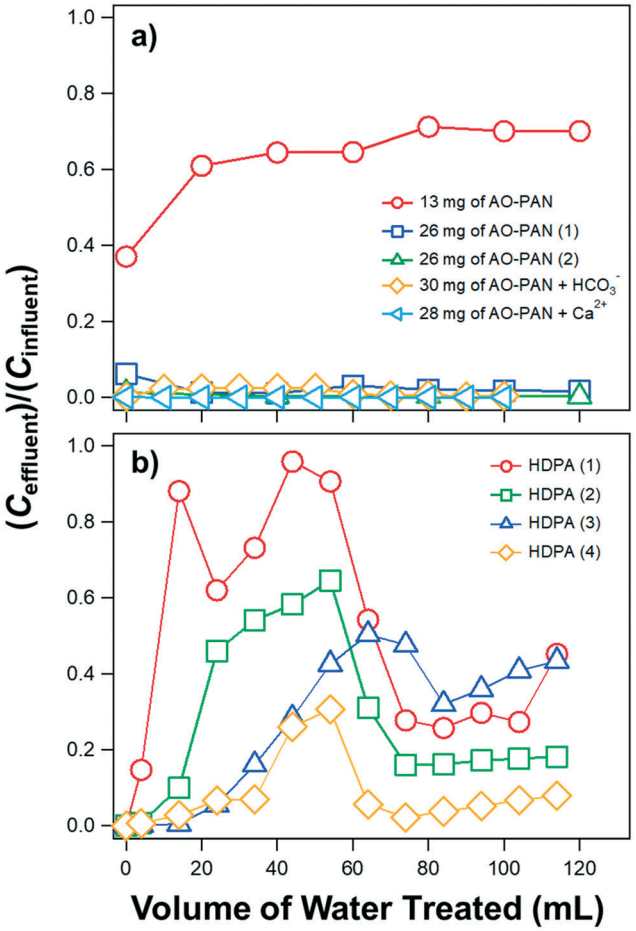

Fig. 5 Normalized concentration (effluent concentration divided by influent concentration) of U^{6+} as a function of the volume treated in a dead-end filtration setup with (a) AO-PAN and (b) 0.5 wt% HDPA-functionalized PAN. Experiments used an influent concentration of 1 μM in 10 mM HEPES (pH 6.8) and a flowrate of 0.8 mL min^{-1} (160 LMH), unless otherwise indicated. For AO-PAN, results are shown for different masses (thicknesses) of filters (13 and 26 mg), replicate filters (1 and 2) and more complex solution chemistries (500 mg L^{-1} of Ca^{2+} or HCO_3^- adjusted to pH 6.8). For HDPA-functionalized materials, four replicate experiments (1 through 4) with 20 mg filters are shown.

For AO-PAN filters, the presence of Ca^{2+} (as a competing ion to simulate hardness) and CO_3^{2-} (as a ligand for uranyl from alkalinity) had no influence on U^{6+} removal (Fig. 5a). Using higher mass filters (26 mg), there was no detectable U^{6+} in the filter effluent across 120 mL of treated volume for either influent solution. Sorbed uranium from the Ca^{2+} and CO_3^{2-} runs were nearly identical to the experiments performed in the absence of competing ions, with U^{6+} contents of ~1.2 μg mg^{-1} for all three trials (as determined by LSC analysis of the reacted filter). The lack of interference from Ca^{2+} and CO_3^{2-} may be due to the chemical complexation of U^{6+} by AO groups on the surface of the mats as opposed to electrostatic interactions that could potentially be impacted by co-solute ions. It should also be noted that the pH of the solution varied from 6.8 to 7.5 over the course of experiments containing the CO_3^{2-} anion, suggesting that some HCO_3^- may have been scavenged by AO-PAN during the run by either amidoxime or residual nitrile groups.

Different behavior was observed in flow through experiments performed with the HDPA-functionalized filters. Results from four replicate experiments are shown in Fig. 5b. Partial U^{6+} removal was observed with each HDPA-containing filter, with detectable U^{6+} in most effluent samples across the four replicate studies. The degree of U^{6+} removal was also highly variable from one experiment to the next, with some systems routinely achieving more than 80% removal of influent U^{6+} (at 1 μM), while much less removal and more rapid breakthrough was observed in other instances. Another noteworthy feature observed in all systems was a period of increasing U^{6+} removal after an initial period of more rapid breakthrough, observed by the clear localized maxima in $C_{effluent}/C_{influent}$ values in each of the four replicate experiments (see maxima after 40–80 mL of treated influent in Fig. 5b).

We propose that these unique U breakthrough profiles result from the mechanism of surface binding responsible for U^{6+} removal in HDPA-filter systems. From pH edge experiments at elevated U^{6+} concentration (10 μM), surface precipitation likely contributes to U^{6+} removal at near-neutral pH values. In contrast, from pH edge experiments at lower initial U^{6+} concentrations (1 μM), more limited removal was observed by HPDA-containing nanofibers at near-neutral pH, with any uptake presumably occurring *via* complexation between the phosphonic acid group on HDPA and soluble U^{6+} species. By analogy, we would expect initial removal in our flow through systems to occur *via* complexation but be relatively limited, consistent with the early periods of U^{6+} breakthrough observed in filter effluent. We would also expect that after some period of filter exposure to influent U^{6+} enough U^{6+} would be bound on the HDPA-functionalized surface to initiate formation of higher order U^{6+} species (*e.g.*, dimers, trimers, oligomers and eventually a separate surface phase). If the rate of formation of these higher order species (resulting from surface bound U^{6+} interacting with dissolved U^{6+} species) is faster than the rate at which available HDPA sites form new surface complexes with dissolved U^{6+} species, we would anticipate the extent of U^{6+} removal in our filter systems to increase over time.

Such a biphasic mechanism for U^{6+} removal (*i.e.*, first HDPA complexing U^{6+} followed by formation of higher order U^{6+} species through bound U-soluble U interactions) would likely explain the high variability observed in break through curves for HDPA-containing filters in Fig. 5b. A critical point in the break through curve will be when formation of higher order surface U^{6+} species begins, and it is likely the occurrence of such a transition point would be dependent on highly localized factors related to the flow path through the nanofiber filter. For example, if we consider the amount of U^{6+} mass accumulated in the filter over time (Fig. S8†), a clear increase in the rate of U^{6+} removal is observed between 40–60 mL of treated influent for all replicates, at which we suspect the transition from U^{6+}-complexation by HDPA to formation of higher order U^{6+} surface species occurs. Notably, however, in all cases, the surface U^{6+} concentration is relatively low (on the order of 1.2 μg mg^{-1} mat or less; see Fig. S8†). Indeed, because of the relatively low loading of surface U^{6+}, far less than observed for U-containing samples previously characterized spectroscopically (see Fig. S5†), we were unable to detect any surface U^{6+} *via* XPS on these reacted filters to further explore differences in bound species as a function of filter run time. We are currently exploring the use of other spectroscopic methods (*e.g.*, XAFS) which may be better suited for examining the nature of bound U^{6+} in HDPA nanofiber filtration systems.

Environmental implications

In this work, we have produced various functionalized nanofibers for binding of U^{6+}. Of the materials we explored, the strongest performance across all system conditions was AO-PAN, which has been widely used for capture of U^{6+} from various matrices. AO-PAN exhibited high U^{6+} capacity and sustained performance during filtration, even in the presence of more complex solution compositions (*e.g.*, hardness and alkalinity). Based on our dead-end filtration experiments, and assuming that the average person consumes 2 L of water daily, our results suggest it would only require 80 g (about 0.2 lbs.) of AO-PAN filter material to treat water contaminated with 1 μM U^{6+} to levels below US EPA standards and our method of detection (*e.g.*, 1 μg L^{-1} *via* our ICP-MS analytical method) for one year.

While other materials exhibited less capacity for U^{6+} uptake, there still may be advantages to these alternative formulations. From a fabrication standpoint, amidoximation requires post-processing of electrospun PAN and uses highly concentrated and harsh reagents. The integration of N- and P-containing surfactants directly into the electrospinning sol gel affords more simplicity in filter fabrication, with less generation of chemical waste. Further, in applications of these materials to sequester and concentrate U^{6+} for biomonitoring or sensing, where information about solution phase speciation may be desirable, the ability to leverage different binding

agents to preferentially sequester separate U^{6+} species may be advantageous. For example, Aq and TBAB were included herein because of the prior use of N-containing functionalities in ion exchange, and thus these surfactants would be well-suited to specifically capture anionic U^{6+} species.

Future work is needed to better understand the nature of surface U^{6+} species on each of the most promising functionalized PAN nanofibers. Herein, the levels of surface-bound U^{6+} generated in our experimental systems prohibited extensive surface characterization. In particular, the mechanism of U^{6+} sorption on HPDA-functionalized nanofibers merits additional investigation based upon results from our flow through systems, which suggest that the surface U^{6+} species may change over time with increasing total U^{6+} bound to the nanofiber surface. Characterization of the bound U^{6+} species on HDPA and other functionalized nanofibers will be important to better predict long-term filter performance, including the potential for inadvertent U^{6+} release during water treatment applications and the potential for filter regeneration and reuse once saturation capacity is achieved.

Conflicts of interest

The authors have no conflicts of interest to declare.

Acknowledgements

Research reported in this work was supported by the National Institute of Environmental Health Sciences of the National Institutes of Health under award number R01ES027145. Additional support for MEC was provided through a National Research Traineeship (NRT) grant from the National Science Foundation (NSF) under award number DGE-1633098 and through an NSF Graduate Research Fellowship. The authors would also like to acknowledge the two anonymous reviewers whose comments improved the clarity and impact of this work.

Notes and references

1 U.S. Environmental Protection Agency, Office of Radiation an dIndoor Air, Radiation Protection Division, *Technical Report on Technologically Enhanced Naturally Occuring Radioactive Materials from uraium Mining Volume 1: Mining and Reclamation Background*, EPA 402-R-08-005, Washington D.C., 2008, Available at: https://www.epa.gov/sites/production/files/2015-05/documents/402-r-08-005-v1.pdf.

2 U.S. Environmental Protection Agency, *Abandoned Uranium Mines (AUM) and the Navajo Nation: Northern Aum Region Screening Assessment Report.; Region 9 Superfund Program*, San Francisco, CA, 2006.

3 K. Moore Dias da Cunha, H. Henderson, B. M. Thomson and A. M. Hecht, Ground water contamination with 238-U, 234-U, 235-U, 226-Ra, and 210-Pb from past uranium mining; cove wash Arizona, *Environ. Geochem. Health*, 2013, **36**, 477–487.

4 U.S. Government Accountability Office, *Uranium Contamination: Overall Scope, Time Frame, and Cost Information is Needed for Contamination Cleanup on the Navajo Rerservation*, GAO-14-323, Washington, D. C., 2014.

5 J. M. Blake, S. Avasarala, K. Artyushkova, A. M. S. Ali, A. J. Brearley, C. Shuey, W. P. Robinson, C. Nez, S. Bill, J. Lewis, C. Hirani, J. S. L. Pacheco and J. M. Cerrato, Elevated Concentrations of U and Co-occurring Metals in Abandoned Mine Wastes in a Northeastern Arizona Native American Community, *Environ. Sci. Technol.*, 2015, **49**, 8506–8514.

6 U.S. Environmental Protection Agency, *National Primary Drinking Water Regulations*, EPA 816-F-09-004, Washinton D. C., 2009. Available at: https://www.epa.gov/sites/production/files/2016-06/documents/npwdr_complete_table.pdf.

7 J. Hoover, M. Gonzales, C. Shuey, Y. Barney and J. Lewis, Elevated Arsenic and Uranium Concentrations in Unregulated Water Sources on the Navajo Nation, USA, *Exposure Health*, 2017, **9**, 113–124.

8 W. M. Murphy and E. L. Shock, Environmental Aqueous Geochemistry of Actinides, in *Uranium: Mineralogy, Geochemistry and the Environment*, ed. P. C. Burns and R. J. Finch, Mineralogical Society of American, Washington, D.C., 1999, vol. 38, pp. 221–254.

9 B. Linhoff, P. Longmire, M. Rearick, D. McQuillan and G. Perkins, Water quality and hydrogeochemistry of a basin and range watershed in a semi-arid region of northern New Mexico, *Environ. Earth Sci.*, 2016, **75**, 13.

10 J. M. Blake, C. L. De Vore, S. Avasarala, A. M. Ali, C. Roldan, F. Bowers, M. N. Spilde, K. Artyushkova, M. F. Kirk, E. Peterson, L. Rodriguez-Freire and J. M. Cerrato, Uranium mobility and accumulation along the Rio Paguate, Jackpile Mine in Laguna Pueblo, NM, *Environ. Sci.: Processes Impacts*, 2017, **19**, 605–621.

11 J. M. Blake, S. Avasarala, A.-M. S. Ali, M. Spilde, J. S. Lezama-Pacheco, D. Latta, K. Artyushkova, A. G. Ilgen, C. Shuey, C. Nez and J. M. Cerrato, Reactivity of As and U co-occurring in Mine Wastes in northeastern Arizona, *Chem. Geol.*, 2019, **522**, 26–37.

12 U.S. Environmental Protection Agency, office of Water, *Point-of-Use or Point-ofEntry Treatment Options for Small Drinking Water Systems*, EPA 815-R-06-010, Washington, D.C., 2006.

13 L. F. Greenlee, D. F. Lawler, B. D. Freeman, B. Marrot and P. Moulin, Reverse osmosis desalination: Water sources, technology, and today's challenges, *Water Res.*, 2009, **43**, 2317–2348.

14 S. Deitz and K. Meehan, Plumbing Poverty: Mapping Hot Spots of Racial and Geographic Inequality in U.S. Household Water Insecurity, *Ann. Am. Assoc. Geogr.*, 2019, **109**, 1092–1109.

15 U.S. Environmental Protection Agency, Providing Safe Drinking Water in Areas with Abandoned Uranium Mines. Navajo Nation: Cleaning Up Abandoned Uranium Mines. Available at: https://www.epa.gov/navajo-nation-uranium-cleanup/providing-safe-drinking-water-areas-abandoned-uranium-mines (accessed September 8, 2019).

16 K. E. Greenstein, N. V. Myung, G. F. Parkin and D. M. Cwiertny, Performance comparison of hematite (α-Fe_2O_3)-polymer composite and core-shell nanofibers as point-of-use

filtration platforms for metal sequestration, *Water Res.*, 2019, **148**, 492–503.

17 K. T. Peter, A. J. Johns, N. V. Myung and D. M. Cwiertny, Functionalized polymer-iron oxide hybrid nanofibers: Electrospun filtration devices for metal oxyanion removal, *Water Res.*, 2017, **117**, 207–217.

18 K. T. Peter, N. V. Myung and D. M. Cwiertny, Surfactant-assisted fabrication of porous polymeric nanofibers with surface-enriched iron oxide nanoparticles: composite filtration materials for removal of metal cations, *Environ. Sci.: Nano*, 2018, **5**, 669–681.

19 K. T. Peter, J. D. Vargo, T. P. Rupasinghe, A. De Jesus, A. V. Tivanski, E. A. Sander, N. V. Myung and D. M. Cwiertny, Synthesis, Optimization, and Performance Demonstration of Electrospun Carbon Nanofiber–Carbon Nanotube Composite Sorbents for Point-of-Use Water Treatment, *ACS Appl. Mater. Interfaces*, 2016, **8**, 11431–11440.

20 J. Kim, C. Tsouris, Y. Oyola, C. J. Janke, R. T. Mayes, S. Dai, G. Gill, L.-J. Kuo, J. Wood, K.-Y. Choe, E. Schneider and H. Lindner, Uptake of Uranium from Seawater by Amidoxime-Based Polymeric Adsorbent: Field Experiments, Modeling, and Updated Economic Assessment, *Ind. Eng. Chem. Res.*, 2014, **53**, 6076–6083.

21 X. Xu, H. Zhang, J. Ao, L. Xu, X. Liu, X. Guo, J. Li, L. Zhang, Q. Li, X. Zhao, B. Ye, D. Wang, F. Shen and H. Ma, 3D hierarchical porous amidoxime fibers speed up uranium extraction from seawater, *Energy Environ. Sci.*, 2019, **12**, 1979–1988.

22 N. Horzum, T. Shahwan, O. Parlak and M. M. Demir, Synthesis of amidoximated polyacrylonitrile fibers and its application for sorption of aqueous uranyl ions under continuous flow, *Chem. Eng. J.*, 2012, **213**, 41–49.

23 G. Lu, A. J. Johns, B. Neupane, H. T. Phan, D. M. Cwiertny, T. Z. Forbes and A. J. Haes, Matrix-Independent Surface-Enhanced Raman Scattering Detection of Uranyl Using Electrospun Amidoximated Polyacrylonitrile Mats and Gold Nanostars, *Anal. Chem.*, 2018, **90**, 6766–6772.

24 M. Sujata Mishra and V. Chakravortty, Extraction of uranium(VI) by the binary mixture of Aliquat 336 and PC88A from aqueous H3PO4 medium, *Hydrometallurgy*, 1997, **44**(3), 371–376.

25 S. Mishra, V. Chakravortty and P. R. V. Rao, Synergistic extraction of uranium(VI) and americium(III) with binary mixtures of Aliquat 336 and PC 88A-TOPO from nitric-sulfuric acid medium, *J. Radioanal. Nucl. Chem.*, 1995, **201**, 325–331.

26 H. Ramebäck and M. Skĺlberg, Separation of neptunium, plutonium, americium and curium from uranium with di-(2-ethylhexyl)-phosphoric acid (HDEHP) for radiometric and ICP-MS analysis, *J. Radioanal. Nucl. Chem.*, 1998, **235**, 229–234.

27 B. Ganguly, Spectroscopic investigation of uranium complexation in the reversed micellar system HDEHP—n-heptane—water, *J. Photochem. Photobiol., A*, 1990, **51**, 401–409.

28 M. M. Aly and M. F. Hamza, A Review: Studies on Uranium Removal Using Different Techniques. Overview, *J. Dispersion Sci. Technol.*, 2013, **34**, 182–213.

29 Eichrom. TRU Resin. https://www.eichrom.com/eichrom/products/tru-resin/ (Accessed September 15, 2019).

30 N. Kenkichi, N. Keiji and M. Utako, On the Mechanism of the Extraction of Uranyl Nitrate by Tributyl Phosphate II. Infrared Study, *Bull. Chem. Soc. Jpn.*, 1960, **33**, 894–898.

31 X. Ye, S. Cui, V. D. Almeida and B. Khomami, Interfacial Complex Formation in Uranyl Extraction by Tributyl Phosphate in Dodecane Diluent: A Molecular Dynamics Study, *J. Phys. Chem. B*, 2009, **113**, 9852–9862.

32 J. C. Crittenden, R. R. Trussell, D. W. Hand, K. J. Howe and G. Tchobanoglous, Membrane Filtration, in *MWH's Water Treatment: Principles and Design*, ed. J. C. Crittenden, R. R. Trussell, D. W. Hand, K. J. Howe and G. Tchobanoglous, 2012.

33 A. Froideval, M. Del Nero, C. Gaillard, R. Barillon, I. Rossini and J. L. Hazemann, Uranyl sorption species at low coverage on Al-hydroxide: TRLFS and XAFS studies, *Geochim. Cosmochim. Acta*, 2006, **70**, 5270–5284.

34 E. Guibal, I. Saucedo, J. Roussy and P. Le Cloirec, Uptake of uranyl ions by new sorbing polymers: discussion of adsorption isotherms and pH effect, *React. Polym.*, 1994, **23**, 147–156.

35 C. Gunathilake, J. Gorka, S. Dai and M. Jaroniec, Amidoxime-modified mesoporous silica for uranium adsorption under seawater conditions, *J. Mater. Chem. A*, 2015, **3**, 11650–11659.

36 N. Pekel, N. Sahiner and O. Guven, Thermodynamics of adsorption of uranyl ions onto amidoximated poly(acrylonitrile)/poly(N-vinyl 2-pyrrolidone) interpenetrating polymer networks, *J. Polym. Sci., Part B: Polym. Phys.*, 2004, **42**, 986–993.

37 T. Hirotsu, S. Katoh, K. Sugasaka, M. Seno and T. Itagaki, Adsorption equilibrium of uranium from aqueous $[UO_2(CO_3)_3]^{4-}$ solution on a polymer bearing amidoxime groups, *J. Chem. Soc., Dalton Trans.*, 1986, 1983–1986.

38 R. Guillaumont, T. Fanghanel, J. Fuger, I. Grenthe, V. Neck, D. A. Palmer and M. H. Rand, *Update on the Chemical Thermodynamics of Uranium, Neptunium, Plutonium, Americium and Technicium*, Elsevier, Amsterdam, 2003, vol. 5.

39 S. D. Kamp and S. J. Morrison, Use of Chemical and Isotopic Signatures to Distinguish Between Uranium Mill-Related and Naturally Occurring Groundwater Constituents, *Ground Water Monit. Rem.*, 2014, **34**, 68–78.

40 D. Gorman-Lewis, P. C. Burns and J. B. Fein, Review of uranyl mineral solubility measurements, *J. Chem. Thermodyn.*, 2008, **40**, 335–352.

41 K. Fujiwara, H. Yamana, T. Fujii, K. Kawamoto, T. Sasaki and H. Moriyama, Solubility product of hexavalent uranium hydrous oxide, *J. Nucl. Sci. Technol.*, 2005, **42**, 289–294.

42 M. Kapnisti, F. Noli, P. Misaelides, G. Vourlias, D. Karfaridis and A. Hatzidimitriou, Enhanced sorption capacities for lead and uranium using titanium phosphates; sorption, kinetics, equilibrium studies and mechanism implication, *Chem. Eng. J.*, 2018, **342**, 184–195.

43 K. L. Cheng, K. Ueno and T. Imamura, *CRC Handbook of Organic Analytical Reagents*, Taylor & Francis, New York, N.Y., 2nd edn, 2017.

44 A. M. Kiwan and R. S. Amin, Solvent-extraction of uranium (IV). 3. Extraction of uranium(IV) by di-(2-ethylhexyl) phosphoric-acid from sulfuric-acid solutions, *J. Inorg. Nucl. Chem.*, 1974, **36**, 2591–2593.

45 M. Riegel, Sorption of Natural Uranium on Weakly Basic Anion Exchangers, *Solvent Extr. Ion Exch.*, 2017, **35**(5), 363–375.

46 J. E. Quinn, M. D. Ogden and K. Soldenhoff, Solvent Extraction of Uranium (VI) from Chloride Solutions using Cyphos IL-101, *Solvent Extr. Ion Exch.*, 2013, **31**, 538–549.

47 A. M. St John, R. W. Cattrall and S. D. Kolev, Extraction of uranium(VI) from sulfate solutions using a polymer inclusion membrane containing di-(2-ethylhexyl) phosphoric acid, *J. Membr. Sci.*, 2010, **364**, 354–361.

48 A. Krestou and D. Panias, Uranium (VI) speciation diagrams in the $UO_2^{2+}/CO_3^{2-}/H_2O$ system at 25 C, *Eur. J. Miner. Process. Environ. Prot.*, 2004, **4**, 113–129.

49 L. Hu, X.-W. Yan, C.-G. Yao, S.-Y. Deng, X.-M. Gao, X.-J. Zhang and D. Shan, Preparation of amidoximated coaxial electrospun nanofibers for uranyl uptake and their electrochemical properties, *Sep. Purif. Technol.*, 2016, **171**, 44–51.

50 D. D. Shao, Y. Y. Li, X. L. Wang, S. Hu, J. Wen, J. Xiong, A. M. Asiri and H. M. Marwani, Phosphate-Functionalized Polyethylene with High Adsorption of Uranium(VI), *ACS Omega*, 2017, **2**, 3267–3275.